

[www.crt-journal.org](http://www.crt-journal.org)

# Crystal Research and Technology

Journal of Experimental and Industrial Crystallography

Zeitschrift für experimentelle und technische Kristallographie

WILEY-VCH

REPRINT

## Angular stability of electric field-induced effects in crystalline materials

O. S. Kushnir\*<sup>1</sup>, O. V. Yurkevych<sup>2</sup>, and A. S. Andrushchak\*\*<sup>3</sup>

<sup>1</sup> Electronics Department, Ivan Franko Lviv National University, P. O. Box 3154, 79054 Lviv-54, Ukraine

<sup>2</sup> Institute of Telecommunications, Radioelectronics and Electronic Engineering, Lviv Polytechnic National University, 12 Bandery St., 79046 Lviv, Ukraine

<sup>3</sup> Faculty of Electrical Engineering, Czestochowa University of Technology, 17 Al. Armii Krajowej PL-42200, Czestochowa, Poland

Received 20 February 2013, revised 20 April 2013, accepted 21 May 2013

Published online 13 June 2013

**Key words** piezoelectric effect, electrooptic effect, lithium niobate, langasite crystals, spatial anisotropy, indicative surfaces.

We analyze angular bandwidths of extrema of the indicative surfaces describing spatial anisotropy of piezoelectric (PE) and electrooptic (EO) properties of doped lithium niobate (LiNbO<sub>3</sub>:MgO) and langasite (La<sub>3</sub>Ga<sub>5</sub>SiO<sub>14</sub>) crystals. A number of highly efficient experimental geometries are suggested, which are promising for PE and EO devices. Our data obtained with both analytical and numerical techniques characterize angular stability of those devices and, in particular, their angular aperture. We show that, besides of a maximal size of the electric field-induced effects, ‘non-direct crystal cuts’ offer considerably higher angular stability of their characteristics, when compared with that typical for ‘direct crystal cuts’ usually employed in PE and EO devices.

© 2013 WILEY-VCH Verlag GmbH & Co. KGaA, Weinheim

### 1 Introduction

Recent advances in optoelectronics, acoustoelectronics and laser techniques, including development of optical modulators and filters, piezoelectric (PE) and electrooptic (EO) devices, adaptive and other components of telecommunications systems are much indebted to a progress of crystalline materials. It is known that physical properties of many crystals vary considerably under external electric, magnetic, mechanical or acoustic fields, so that the corresponding effects, such as PE, EO, magneto-optic or acousto-optic, may be promising for different applications. The efforts in this direction have been undertaken mainly in order to (i) search for new crystals and improve their growth technologies enabling synthesis of highly efficient optoelectronic or acoustoelectronic materials and/or (ii) increase efficiency of crystalline materials by optimizing geometry of PE, EO or acousto-optic coupling.

The latter point appears to be of a primary importance for a large number of low-symmetry crystalline materials, for which relevant analysis of anisotropy of external field-induced effects and a proper choice of geometry of PE or EO cells may considerably improve the efficiency and performance characteristics of the devices. A number of techniques have been suggested for this aim (see, e.g., Refs. [1–12]). As a matter of fact, they deal with so-called indicative surfaces (ISs) that describe spatial anisotropy of an external field-induced effect subjected to analysis (the simplest example of an IS for a second-rank optical gyration tensor may be found in the textbook [13]). One should start from a complete set of nonzero tensor components  $r_{\eta_1 \dots \eta_N}$  ( $N$  being the rank of the tensor) describing a given effect for some material, which are supposed to be already known from experiment. Then one can construct the IS as a surface  $r(\theta, \varphi)$  for which the distance  $r$  from the origin to a given point defined by spherical angles  $\theta$  and  $\varphi$  is equal to the size of the effect along a given direction (e.g., an effective EO coefficient or acousto-optic figure of merit – see [6,9,11]). Notice that spatial directions of the external field, the propagation and polarization directions of light (or acoustic) waves should be predetermined

\*Corresponding author: e-mail: o\_kushnir@franko.lviv.ua

\*\*e-mail: anat@polynet.lviv.ua

for each of the ISs under interest (e.g., these directions may be chosen to be parallel or perpendicular to the radius vector of the IS – see discussion below). Then a numerical analysis of the IS would result in maximal magnitudes of the tensorial effect and angular orientations  $\theta_{0i}, \varphi_{0i}$  ( $i = 1, 2, \dots$ ) of these extrema, thus providing optimized experimental geometries, which ensure maximal efficiency possible for a given crystalline material.

In relation to the above analysis, there arises an additional problem concerned with changes in size of the field-induced effects in the vicinity of their extrema, which occur with changing field or light propagation directions, temperature of material or frequency of the field (or the light). In fact, these factors will define angular, temperature or frequency stability of these extrema. The simplest example is ‘angular bandwidth’ of the maximum of a field-induced effect, which would finally govern the angular aperture of a relevant device in case if an optical effect is dealt with. Nonetheless, the problem has not been properly considered in the literature, although it seems to be crucial for many applications. Indeed, the direction of electric field applied to a crystal can be set with a finite accuracy only; any laser beam is characterized by some angular divergence, while practical procedures of orientation of single crystals can also involve some errors. Then, if a spatial extremum (a maximum if we mean the absolute magnitude) of the effect is narrow enough and the corresponding effective tensorial coefficient reveals ‘sharp’ angular behavior (i.e., drops significantly in a close enough angular vicinity of the maximum), any practical utilization of such a highly efficient crystalline cut may prove to be questionable.

The goal of this work is to present a general approach for the analysis of angular stability of the size of field-induced effects in anisotropic media. As particular examples, we demonstrate this analysis for the two effects, PE and EO, and two different crystalline materials, MgO-doped lithium niobate ( $\text{LiNbO}_3:\text{MgO}$ ) and langasite ( $\text{La}_3\text{Ga}_5\text{SiO}_{14}$ ). Likewise its undoped counterpart  $\text{LiNbO}_3$ ,  $\text{LiNbO}_3:\text{MgO}$  represents a material well known by its numerous electronic, optoelectronic and acoustoelectronic applications, and, moreover, it reveals higher radiation hardness enabling applications that involve a powerful laser radiation [11,12,14–16]. Though studied in much less detail, the  $\text{La}_3\text{Ga}_5\text{SiO}_{14}$  compound is known [17,18] to have very high thermal stability of its PE properties, which can be important for different applications.

## 2 Basic concept and methodology

The value  $r$  characterizing any field-induced physical effect depends at least on the angular coordinate  $\alpha$  (we use it for conciseness instead of the set  $\alpha = (\theta, \varphi)$ ), which implies spatial anisotropy of the effect, the frequency  $\omega$  of the field (or, alternatively, that of the light), and the temperature  $T$  of the material. Let the dependence  $r(\alpha, \omega, T)$  represent the IS constructed at certain working frequency  $\omega^*$  and temperature  $T^*$ . Let us assume that an angular extremum  $r$  of the induced effect,  $r_{\max}$ , occurs at some  $\alpha_0 = \alpha_0(\omega^*, T^*)$ . In a close enough vicinity of this extreme direction, the  $r$  value as a function of  $\alpha, \omega$  and  $T$  can be expressed as a power series

$$r(\alpha, \omega, T) \approx r(\alpha_0, \omega^*, T^*) + \left. \frac{\partial r}{\partial \alpha} \right|_{\alpha=\alpha_0} (\alpha - \alpha_0) + \frac{1}{2!} \left. \frac{\partial^2 r}{\partial \alpha^2} \right|_{\alpha=\alpha_0} (\alpha - \alpha_0)^2 + \left. \frac{\partial r}{\partial \omega} \right|_{\omega=\omega^*} (\omega - \omega^*) + \frac{1}{2!} \left. \frac{\partial^2 r}{\partial \omega^2} \right|_{\omega=\omega^*} (\omega - \omega^*)^2 + \left. \frac{\partial r}{\partial T} \right|_{T=T^*} (T - T^*) + \frac{1}{2!} \left. \frac{\partial^2 r}{\partial T^2} \right|_{T=T^*} (T - T^*)^2 + \dots, \quad (1)$$

in which higher-order terms in the deviations from the  $\alpha_0, \omega^*$  and  $T^*$  points have been dropped. For convenience, we rewrite Eq. (1) as

$$r(\alpha, \omega, T) \approx r(\alpha_0, \omega^*, T^*) + \gamma_\alpha^{(1)} (\alpha - \alpha_0) + \gamma_\alpha^{(2)} (\alpha - \alpha_0)^2 + \gamma_\omega^{(1)} (\omega - \omega^*) + \gamma_\omega^{(2)} (\omega - \omega^*)^2 + \gamma_T^{(1)} (T - T^*) + \gamma_T^{(2)} (T - T^*)^2 + \dots, \quad (2)$$

where, following the work [19], we have introduced angular ( $\gamma_\alpha$ ), spectral ( $\gamma_\omega$ ) and temperature ( $\gamma_T$ ) dispersive coefficients of the first (superscript ‘(1)’) and second (superscript ‘(2)’) orders.

It is important that the angular coefficient of the first order,  $\gamma_\alpha^{(1)}$ , equals to zero as far as we work in the vicinity of the extreme direction  $\alpha_0$  ( $r(\alpha_0) = r_{\max}$ ). Moreover, in a rough approximation one can ignore the quadratic dispersive coefficients  $\gamma_\omega^{(2)}$  and  $\gamma_T^{(2)}$ , while recalling that the linear coefficients  $\gamma_\omega^{(1)}$  and  $\gamma_T^{(1)}$  should not in general be equal to zero. Therefore a deviation of size of the induced effect from its extremum reads as

$$r(\alpha, \omega, T) - r_{\max}(\alpha_0, \omega^*, T^*) \approx \gamma_\alpha^{(2)} (\alpha - \alpha_0)^2 + \gamma_\omega^{(1)} (\omega - \omega^*) + \gamma_T^{(1)} (T - T^*) + \dots. \quad (3)$$

In what follows, we will restrict our general approach only to dependence of the effect on the angular coordinates and will disregard its additional dependences on the frequency and temperature. It is evident that, in any practical situation, zero angular dispersive coefficient  $\gamma_\alpha^{(1)}$  should mean high angular stability of the effect size.

Such a statement seems to be somewhat surprising in one aspect. Indeed, it is well known from previous studies (see, e.g., [6,12]) that the angular orientations of extrema of the ISs often correspond to so-called ‘indirect crystal cuts’, i.e. to spatial directions different from the principal (crystallophysical) axes  $X_1$ ,  $X_2$  and  $X_3$  (i.e., at least one of the angles  $\theta$  and  $\varphi$  does not equal to 0,  $90^\circ$ ,  $180^\circ$ , etc.). From the other hand, one can remind that angular changes of many optical parameters such as, e.g., refractive indices and absorption coefficients, which are related to a second-rank dielectric impermeability tensor, are sharp for any ‘indirect crystal cuts’. In other words, these optical properties are critical to small angular changes in the vicinity of  $\alpha_0$ , contrary to what has been stated for the external field-induced properties. However, this situation is because the principal axes of the Fresnel ellipsoid necessarily coincide with the mutually orthogonal principal axes  $X_1$ ,  $X_2$  and  $X_3$ , at least for orthorhombic or higher crystal symmetries. Therefore the extrema in the angular dependences of the refractive indices will be observed only for the directions  $X_1$ ,  $X_2$  and  $X_3$ , which are associated with the direct crystal cuts, and noncritical changes will be peculiar for their close angular vicinity. On the contrary, the field-induced effects are described by the tensors of higher (third or fourth) ranks. The symmetry implications for these tensors are much more complicated and they do not forbid the appearance of extrema and noncritical angular behavior for the indirect cuts (see the results [9–11] and the analysis given in subsection 3.1).

Hence, apart from an extreme size of the induced effects associated with the indirect crystal cuts, there is another advantage of those experimental geometries, a noncritical angular behavior of the effect in the vicinity of its extrema. This implies rather weak changes in the size of the effect due to (accidental or intentional) deviations from the optimized directions of external field or light propagation and polarization. This fact, which has so far remained unnoticed, seems to be crucial in designing many PE, EO, acoustooptic or some other devices. In case of field-induced optical effects, it should significantly increase the angular aperture of the corresponding devices.

There is also a close analogy of the phenomena considered above with practically important noncritically phase-matched nonlinear optical geometries (see, e.g., [19–23]). In particular, it is well known that a so-called non-critical phase matching condition can be achieved at  $\theta_0 = 90^\circ$  and some fundamental frequency and temperature, resulting in a zero first-order angular dispersive coefficient  $\gamma_\theta^{(1)}$  for the phase mismatch function  $\Delta k = \Delta k(\theta)$ . The consequence is that the angular bandwidth of the phase-matching curve  $\Delta k(\theta)$  for the second harmonic generation can be as large as several angular degrees. This differs drastically from the usual geometries of critical phase matching, when typical tolerable deviations are of the order of angular minutes or even seconds. The analysis in terms of this work can testify that the above noncriticality is just because the function  $\Delta k(\theta)$  reaches its extremum at  $\theta_0$  (notice that we have again the case of a direct crystal cut,  $\theta_0 = 90^\circ$ , as should be with the properties associated with the refractive indices – see the discussion above).

### 3 ISs of PE and EO properties of $\text{LiNbO}_3:\text{MgO}$ and $\text{La}_3\text{Ga}_5\text{SiO}_{14}$ crystals and angular bandwidths of their extrema

In this section we present both a partial analytical analysis and a complete numerical study of several typical examples of ISs for the PE and EO effects in MgO-doped lithium niobate ( $\text{LiNbO}_3:\text{MgO}$ , the point symmetry class  $3m$ ) and langasite ( $\text{La}_3\text{Ga}_5\text{SiO}_{14}$ , the symmetry class 32) crystals, with the emphasis on angular dependences of these effects and angular stability of their extrema.

**3.1 Basic relationships for the ISs** We will illustrate the main principles of construction of ISs for higher-order tensors on the example of direct PE effect described by a third-rank tensor  $d_{\eta\mu\nu}$ , of which internal symmetry  $d_{\eta\mu\nu} = d_{\eta\nu\mu}$  strictly follows from its definition ( $E_\eta = d_{\eta\mu\nu}^* S_{\mu\nu}$ , with  $S_{\mu\nu}$  being the mechanical stress tensor). Unlike the second-rank tensors of which anisotropy is completely represented by a single IS (see [13]), the number of ISs describing anisotropy of higher-order effects is, in principle, infinite. This is because the directions of the electric field and the mechanical strains (for the case of PE effect) or those of the electric field and the propagation and polarization of light (for the case of EO effect) can be arbitrarily oriented with respect to each other. Here it would be reasonable to restrict consideration only to the most practical ‘parallel’ or ‘orthogonal’ experimental geometries, for which the above mentioned directions are kept parallel or orthogonal.

One of such geometries corresponds to a so-called longitudinal PE: we consider a (spatially varying) value of the effect for the case when both the electric field and the (compressing) mechanical stress are applied parallel

to each other and to the direction in which we find the effect value (see [13]). If, for the sake of concreteness, the above direction is initially defined by the principal axis  $X_1$ , we would deal with the tensor component  $d_{111}$ . Passing to some other spatial direction specified by the direction cosines  $c_{\eta\mu}$ , under condition of invariable mutual orientation of the electric field and the mechanical stress, one can describe the effect value in the rotating coordinate system  $X'_1X'_2X'_3$  with a standard relation  $d'_{111} = c_{1\eta}c_{1\mu}c_{1\nu}d_{\eta\mu\nu}$  [13].

To track completely spatially varying effect size, it would be appropriate to use formally the same relation  $d'_{111}(\theta, \varphi) = c_{1\eta}(\theta, \varphi)c_{1\mu}(\theta, \varphi)c_{1\nu}(\theta, \varphi)d_{\eta\mu\nu}$ , though with the direction cosines depending on the spherical coordinates  $\theta$  and  $\varphi$ . Now the tensorial indices '111' in the scalar quantity  $d'_{111}(\theta, \varphi)$  are of no significance – one could equally rightly denote them as  $d'_{222}(\theta, \varphi)$  or  $d'_{333}(\theta, \varphi)$  or omit them, since the system  $X'_1X'_2X'_3$  rotates all the same. The parameter  $d'_{111}(\theta, \varphi)$  referred to as 'a longitudinal IS of PE effect' [13] may now be quite conventionally labeled as  $d_{EE}^S$ , where the superscript 'S' indicates that the radius-vector  $\mathbf{r}$  of the IS is parallel to the direction  $S$  of piezo-induced (for simplicity, uniaxial compression) stress, whereas the same subscripts 'EE' symbolize the fact that the  $S$  and  $\mathbf{E}$  directions remain the same. In other words, all the information regarding specific character of the given IS is contained in the relations  $\mathbf{r} \parallel \mathbf{E} \parallel S$ . Of course, there exist infinitely many other ISs of the PE effect dealing with the other experimental geometries, e.g. an IS  $d_{ES}^E$ , for which we have  $\mathbf{r} \parallel \mathbf{E}$  and the stress is kept perpendicular to the field ( $S \perp \mathbf{E}$ ).

As specific practical examples, below we will consider only several ISs:  $d_{EE}^S(\mathbf{r} \parallel \mathbf{E} \parallel S)$ ,  $d_{ES}^E(\mathbf{r} \parallel \mathbf{E}, S \perp \mathbf{E})$  and  $d_{ES}^p(\mathbf{r} \parallel \mathbf{p} \perp \mathbf{E}, \mathbf{r} \perp S, S \perp \mathbf{E})$  for the effective PE coefficient, and  $\delta\Delta_{EE}^i(\mathbf{r} \parallel \mathbf{E} \parallel \mathbf{i})$ ,  $\delta\Delta_{Ej}^E(\mathbf{r} \parallel \mathbf{E}, \mathbf{E} \perp \mathbf{j})$  and  $\delta\Delta_{Ei}^i(\mathbf{r} \parallel \mathbf{i}, \mathbf{E} \perp \mathbf{i})$  for the electrically induced optical path change due to the EO effect (see, e.g., [27]). The latter parameter refers to the unit crystal thickness and unit electric field and is defined as  $\delta\Delta = -r_{eff}n_{eff}^3 + 2(n_{eff} - 1)d_{eff}$ , where  $r_{eff}$  and  $d_{eff}$  denote the effective EO and PE coefficients for a given experimental geometry (e.g.,  $d_{eff}$  is given by one of the ISs just listed), and  $n_{eff}$  implies the effective refractive index specified for this geometry. Notice that the optical path change is concerned, in the first place, with interferometric applications of the EO effect (cf. with the electrically induced phase retardation addressed to in the work [11]). As for the conventional notations of these ISs not explained earlier, the vector  $\mathbf{p}$  is normal to both of the  $S$  and  $\mathbf{E}$  directions, while  $\mathbf{i}$  and  $\mathbf{j}$  are the polarization vectors of respectively the extraordinary and ordinary light waves in crystal (the propagation vector  $\mathbf{k}$  being orthogonal to  $\mathbf{i}$  and  $\mathbf{j}$ ). Notice also that the EO ISs under our interest are just those associated with possible practical influence of piezoelectricity upon electrooptics.

Omitting all the calculation details (see [11,25,27]), we present only final formulae for the ISs mentioned above. The first example concerned with the symmetry class  $3m$  (i.e., lithium niobate crystals) is

$$d_{EE}^S(\theta, \varphi) = -d_{22}\sin^3\theta\sin 3\varphi + (d_{31} + d_{15})\sin^2\theta\cos\theta + d_{33}\cos^3\theta, \quad (4)$$

$$d_{ES}^E(\theta, \varphi) = -d_{22}\sin\theta\cos^2\theta\sin 3\varphi + d_{31}\cos^3\theta + (d_{33} - d_{15})\sin^2\theta\cos\theta, \quad (5)$$

$$d_{ES}^p(\theta, \varphi) = -d_{22}\cos^2\theta\cos 3\varphi, \quad (6)$$

$$\begin{aligned} \delta\Delta_{EE}^i(\theta, \varphi) = & [r_{22}\sin^3\theta\sin 3\varphi - (r_{13} + 2r_{51})\sin^2\theta\cos\theta - r_{33}\cos^3\theta] (n_o^{-2}\sin^2\theta + n_e^{-2}\cos^2\theta)^{-3/2} \\ & + 2[(n_o^{-2}\sin^2\theta + n_e^{-2}\cos^2\theta)^{-1/2} - 1][ -d_{22}\sin\theta\cos^2\theta\sin 3\varphi + d_{31}\cos^3\theta \\ & + (d_{33} - d_{15})\sin^2\theta\cos\theta], \end{aligned} \quad (7)$$

$$\begin{aligned} \delta\Delta_{Ej}^E(\theta, \varphi) = & -(r_{22}\sin\theta\sin 3\varphi + r_{13}\cos\theta)n_o^3 \\ & - 2(n_o - 1)[d_{22}\sin\theta\cos^2\theta\sin 3\varphi - d_{31}\cos^3\theta - (d_{33} - d_{15})\sin^2\theta\cos\theta]. \end{aligned} \quad (8)$$

The second example for the case of symmetry class  $32$  (i.e., langasite crystals) is given by

$$d_{ES}^p(\theta, \varphi) = \frac{1}{2}d_{14}\sin 2\theta - d_{11}\cos^2\theta\sin 3\varphi, \quad (9)$$

$$\begin{aligned} \delta\Delta_{Ei}^i(\theta, \varphi) = & (r_{41}\sin 2\theta + r_{11}\sin^2\theta\sin 3\varphi) (n_o^{-2}\sin^2\theta + n_e^{-2}\cos^2\theta)^{-3/2} \\ & + 2[(n_o^{-2}\sin^2\theta + n_e^{-2}\cos^2\theta)^{-1/2} - 1] \left( \frac{1}{2}d_{14}\sin 2\theta - d_{11}\cos^2\theta\sin 3\varphi \right), \end{aligned} \quad (10)$$

Here  $d_{lm}$  ( $l \equiv \eta = 1 \dots 3$  and  $m \equiv \mu\nu = 1 \dots 6$ ) and  $r_{lm}$  ( $l \equiv \eta\mu = 1 \dots 6$  and  $m \equiv \nu = 1 \dots 3$ , since  $r_{\eta\mu\nu} = r_{\mu\eta\nu}$ ) are respectively the tensorial coefficients of the inverse PE and EO effects written in the matrix notation, whereas  $n_o$  and  $n_e$  imply the refractive indices for the ordinary and extraordinary light waves. We are also to stress that Eqs. (4)–(10) are a good illustration of the fact that the higher-order physical effects in crystals are always dependent on both the polar ( $\theta$ ) and azimuthal ( $\varphi$ ) angles, even in optically uniaxial crystals. This is unlike the natural optical anisotropy which is uniquely described by a single polar angle between the wave vector  $\mathbf{k}$  of light and the optic axis  $X_3$ .

Relations (4)–(10) show that the angular orientations  $\theta_0$  and  $\varphi_0$  of extrema of the field-induced effects are determined by competition of different tensor components  $d_{lm}$  (or  $r_{lm}$ ). Closer inspection of formulae (4)–(10) also testifies that, in general, the  $\theta_0$  and  $\varphi_0$  angles can differ from  $0$ ,  $90^\circ$  or  $180^\circ$ . Of course, besides of material-dependent magnitudes and signs of  $d_{lm}$  (or  $r_{lm}$ ), the orientation of the extrema must be governed by the general symmetry requirements. According to the von Neumann's principle, the IS should involve all the symmetry elements of a point class describing a given material ( $3m$  and  $32$  for the cases of lithium niobate and langasite). In particular, the orientations  $\varphi_{0i}$  of different extrema (numbered by the index  $i$ ) should necessarily be linked by the rotations associated with the three-fold axis  $X_3$ . The extrema can occur at either  $\theta_0 = 0$  ( $180^\circ$ ) or  $\theta_0 \neq 0$ . Here the former case is degenerate, while the latter corresponds to three different angles  $\varphi_{0i}$  divided by the angular distance  $120^\circ$ . Moreover, if the extremum indeed occurs at  $\theta_0 \neq 0$  in the upper semisphere ( $0 < \theta_0 < 90^\circ$ ), then the symmetry of the class  $3m$  would dictate availability of another extremum in the lower semisphere ( $90^\circ < \theta_0 < 180^\circ$  – see also specific examples of ISs shown in figure 1(a), (b), figure 3(a), (b), and figure 4(a), (b)).

Of all these considerations, the most important is that the extrema of the field-induced effects can occur at least at  $\theta_0 \neq 0$ ,  $90^\circ$ ,  $180^\circ$ . Irrespective of the  $\varphi_0$  value, this clearly corresponds to what we call as ‘indirect cuts’.

**3.2 Analytical analysis of the PE ISs and their angular bandwidths** Now let us analyze the IS given by Eq. (4), using the general approach to angular stability of the field-induced effects presented in Section 2. The extrema of this IS may be found from the conditions of zero partial derivatives,  $\partial d_{EE}^S(\theta, \varphi)/\partial\theta = 0$  and  $\partial d_{EE}^S(\theta, \varphi)/\partial\varphi = 0$ . These lead respectively to

$$\sin\theta = 0, a \tan^2\theta + b(\varphi) \tan\theta + c = 0, \quad (11)$$

$$\sin^3\theta \cos 3\varphi = 0, \quad (12)$$

where  $a = d_{31} + d_{15}$ ,  $b(\varphi) = 3d_{22} \sin 3\varphi$  and  $c = 3d_{33} - 2d_{31} - 2d_{15}$ . Applying standard verifying mathematical procedures, we find that one of the possible maximums appears at the spherical angles  $\theta_0 = \arctan[(b(\varphi) + \sqrt{b^2(\varphi) - 4ac})/(2a)]$  and  $\varphi_0 = 90^\circ$ . Taking the experimental  $d_{lm}$  values measured in the study [15] for the MgO-doped lithium niobate ( $d_{15} = 66.6$ ,  $d_{22} = 19.2$ ,  $d_{31} = 0.4$  and  $d_{33} = 4.1$  pm/V), we obtain  $\theta_0 \approx 61.4^\circ$ . In other words, the extremal value of the PE effect takes place just for an indirect crystal cut. The maximum itself,  $d_{EE,\max}^S$ , is equal to 38.2 pm/V. Notice that these figures agree fairly well with the optimal angles  $\theta_0$ ,  $\varphi_0$  and the IS maximum derived using a further numerical analysis (see subsection 3.2 and table 1 below). Remembering that we deal here with the angular set  $\alpha = (\theta, \varphi)$ , we are to introduce the two angular dispersive coefficients of the first order,  $\gamma_\theta^{(1)}$  and  $\gamma_\varphi^{(1)}$ , which should be zero under these conditions.

The calculations of the second-order angular dispersive coefficients  $\gamma_\theta^{(2)}$ ,  $\gamma_{\theta\varphi}^{(2)}$  and  $\gamma_\varphi^{(2)}$ , using second-order partial derivatives of the function  $d_{EE}^S(\theta, \varphi)$  (see Eqs. (1) and (3)), yield in

$$2\gamma_\theta^{(2)} = \partial^2 d_{EE}^S(\theta, \varphi)/\partial\theta^2 = -\frac{1}{2}[(3a - c) \sin\theta + b(\varphi) \cos\theta] \sin 2\theta - [b(\varphi) \sin\theta + c \cos\theta] \cos 2\theta, \\ \gamma_{\theta\varphi}^{(2)} = \partial^2 d_{EE}^S(\theta, \varphi)/\partial\theta\partial\varphi = -3b(\varphi) \sin^2\theta \cos\theta \cot 3\varphi, \quad 2\gamma_\varphi^{(2)} = \partial^2 d_{EE}^S(\theta, \varphi)/\partial\varphi^2 = 3b(\varphi) \sin^3\theta. \quad (13)$$

With the experimental values of PE coefficients, we get  $\gamma_\theta^{(2)} \approx -83.4$ ,  $\gamma_{\theta\varphi}^{(2)} = 0$  and  $\gamma_\varphi^{(2)} \approx -58.5$  pm/V. Of course, the sufficient condition of an extremum of function of two variables  $\theta$  and  $\varphi$  expressed in terms of the dispersive coefficients ( $\gamma_\theta^{(2)}\gamma_\varphi^{(2)} - 4[\gamma_{\theta\varphi}^{(2)}]^2 > 0$ ) is fulfilled and, moreover, here we deal just with a maximum ( $\gamma_\theta^{(2)}, \gamma_\varphi^{(2)} < 0$ ).

Now let us proceed to analyzing the angular bandwidth of the spatial extrema appearing on the IS. The first question concerns a relevant quantitative parameter to be chosen in order to characterize this bandwidth. As a practical way out, one can use a solid angle around the maximum, in which the size of the effect, as described by the IS, drops down not more than a certain predetermined amount, when compared with the maximal value

(e.g., not more than 10 per cent). In particular, the angular width of laser beams is often specified in such a way (see, e.g., [24]). In a similar manner, one can also define the appropriate angular region  $\delta\theta = \theta - \theta_0$  (at a given  $\varphi$  value, e.g., at the optimal  $\varphi_0$  one) and the region  $\delta\varphi = \varphi - \varphi_0$  (at an optimum  $\theta_0$  value), where the effect is ‘stable’ enough, e.g. not less than 90 per cent of the maximum. Then the formula

$$r(\theta, \varphi) - r_{\max}(\theta_0, \varphi_0) \approx \gamma_{\theta}^{(2)}\delta\theta^2 + \gamma_{\theta\varphi}^{(2)}\delta\theta\delta\varphi + \gamma_{\varphi}^{(2)}\delta\varphi^2 + \dots, \quad (14)$$

which strictly follows from Eq. (3), may be applied, with  $r(\theta, \varphi) = 0.9r_{\max}(\theta_0, \varphi_0)$ . Using the dispersive coefficients known for the IS  $d_{EE}^S(\theta, \varphi)$ , we get  $\delta\theta \approx 12.3^\circ$  (at  $\varphi_0 = 90^\circ$  and  $\delta\varphi = 0$ ) and  $\delta\varphi \approx 14.6^\circ$  (at  $\theta_0 \approx 61.4^\circ$  and  $\delta\theta = 0$ ), again in fair agreement with the data obtained with the numerical methods ( $\delta\theta \approx -12 \div +13^\circ$  and  $\delta\varphi \approx \pm 15^\circ$  – see table 1 below). Notice that the relevant figures are very high. In fact, one can say of a huge stability of the maximums of the PE effect described by the IS  $d_{EE}^S(\theta, \varphi)$ , since one loses only 10 per cent of the effect size while the electric field direction deviates as large as  $\sim 25 - 30^\circ$ . Our further analysis will prove that the same remains true of the other ISs, thus confirming practical advantages of the indirect cuts of crystals revealing maximal PE or EO effects.

In principle, a similar analysis can be performed for another IS  $d_{ES}^p(\theta, \varphi)$  of the PE effect (see Eq. (6)<sup>i</sup>). However, any general analytical analysis of angular bandwidths of the IS maxima is hindered in many aspects. It is dependent on both the point symmetry class and specific values of the tensor coefficients, which are different for different materials. Moreover, this analysis becomes very complicated in many cases. For instance, this is true of the IS  $d_{ES}^E(\theta, \varphi)$  given by Eq. (5), since the condition of zero partial derivative over the  $\theta$  variable results in a cubic equation with parameters. For this reason, further on we will consider stability of the IS maxima, using simpler and more universal numerical approaches.

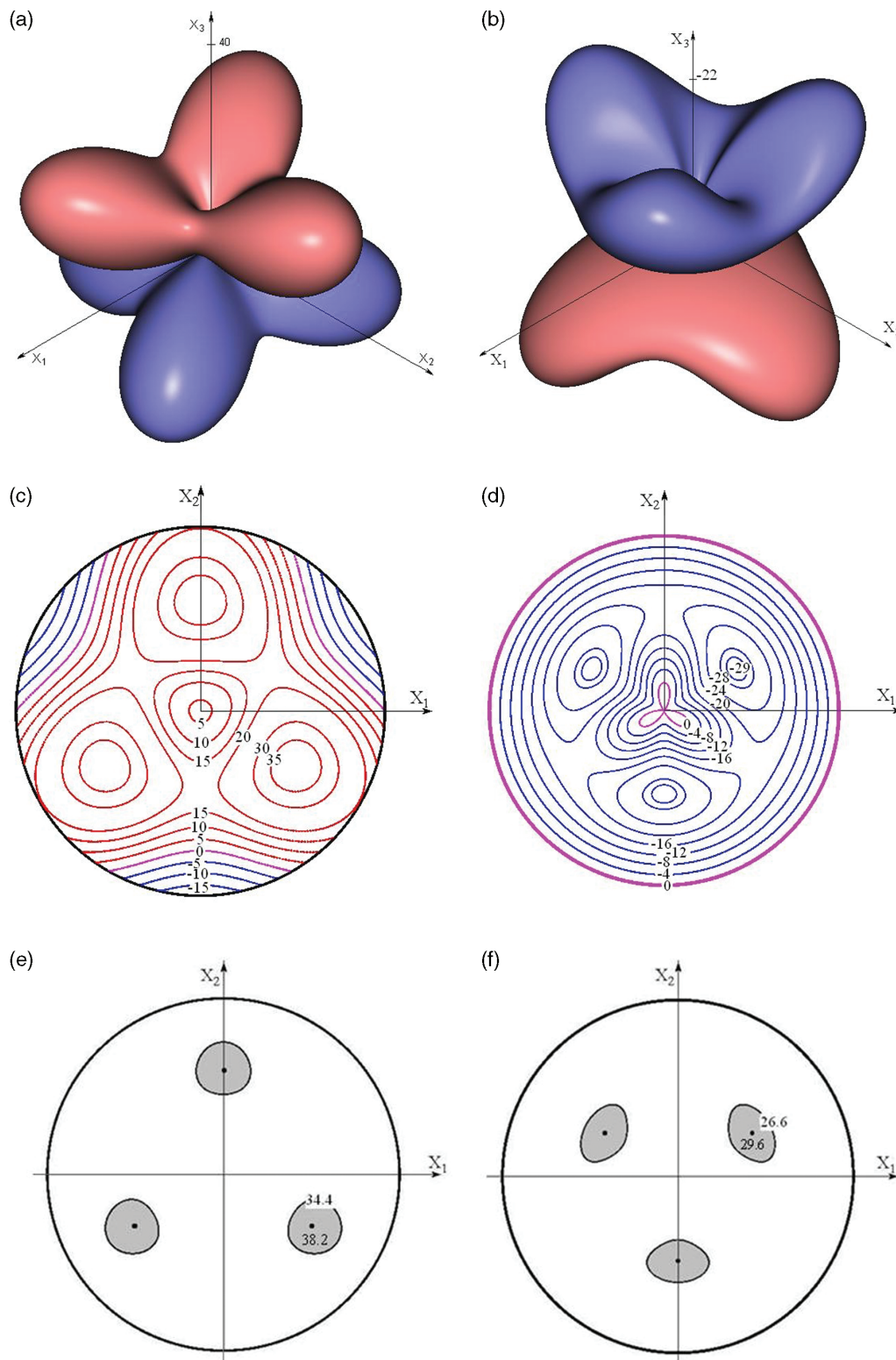
**3.3 Numerical results for LiNbO<sub>3</sub>:MgO** Our analysis of angular stability of the PE and EO parameters for the LiNbO<sub>3</sub>:MgO crystals has been based on the experimental results for the PE constants [15] (see the data introduced above), the EO coefficients ( $r_{13} = 10.9$ ,  $r_{22} = 7.5$ ,  $r_{33} = 34.3$  and  $r_{51} = 34.9$  pm/V [26]), and the room-temperature refractive indices measured at the wavelength of 633 nm ( $n_o = 2.2841$  and  $n_e = 2.1994$  – see [26]). Basing on those data and using our original software Calc3D, we have constructed the ISs described by Eqs. (4)–(8). Then the angular intervals  $\delta\theta$  and  $\delta\varphi$  where the effects are stable enough have been determined, while applying computer-based methods of analysis and using well-known techniques of stereographic projections of the ISs (e.g., the Wulff nets).

Figure 1 shows the ISs  $d_{EE}^S$  and  $d_{ES}^E$  (panels (a) and (b)) of the PE effect in LiNbO<sub>3</sub>:MgO, their stereographic projections on the  $X_1X_2$  plane (panels (c) and (d)), and less detailed stereographic projections with the marked regions around the IS extrema, where the effect size is not less than 90 per cent of the extrema (panels (e) and (f)). Numbers in figure 1, figure 3 and figure 4 indicate the values corresponding to different contour lines or the extrema of the ISs. Notice that the ISs can acquire both positive and negative values, which are indicated respectively in red and blue in the color versions of figure 1, figure 3 and figure 4 (see also marking of the contour lines). Table 1 lists extremal values peculiar for the ISs of the PE effect, including the IS  $d_{ES}^p$  not represented in figure 1, along with corresponding optimal spherical angles  $\theta_0$  and  $\varphi_0$ . This provides valuable information about optimized experimental PE geometries for the lithium niobate crystals, which are characterized by the highest PE efficiency (see figure 2) and can be employed, e.g., while constructing PE transducers.

Closer examination of the PE ISs proves that, in case of the transverse PE effect ( $\mathbf{E} \perp S$ ), the efficiency of the indirect crystal cut (see figure 2(b) and the second row in table 1) is about 1.5 times higher than that corresponding to the most efficient of the direct-cut geometries ( $\mathbf{E} \parallel X_2$  and  $S \parallel X_1$ ). The advantage of indirect crystal cuts is even larger in case of the longitudinal PE effect: here the best direct cut ( $\mathbf{E} \parallel S \parallel X_2$  – see figure 1(a)) exhibits twice as lower efficiency when compared to the optimal indirect cut (see figure 2(a) and the first row in table 1). This advantage will become significantly greater if we pass from the amplitude-related parameters such as  $\mathbf{E}$ ,  $\mathbf{d}$ , etc. to power-related ones which are quadratic in the former parameters.

To characterize quantitatively angular bandwidths of the extrema of the ISs for LiNbO<sub>3</sub>:MgO, we have applied the technique of stereographic projections (see figure 1(e) and (f)). As mentioned above, we have determined angular ‘regions of stability’ of the extrema of the induced effects, using the criterion that the effect in the vicinity of its extremum should not drop down by more than 10 per cent. In particular, the regions of angular stability of the longitudinal and transverse PE effects are marked by shading respectively in panels (e) and (f) of figure 1. Assume

<sup>i</sup>Notice that, as a rare exception, here the PE effect achieves its angular maximum for the direct crystal cuts (e.g., at  $\theta_0 = 0^\circ$  and  $\varphi_0 = 180^\circ$  – see also the numerical data in table 1).



**Fig. 1** (a), (b) ISs of PE effect in  $\text{LiNbO}_3:\text{MgO}$  crystals; (c), (d) their stereographic projections; (e), (f) stereographic projections with shaded angular bandwidths of the IS extrema (see explanations in text). Panels (a), (d) (e) and (b), (d), (f) correspond respectively to longitudinal ( $\mathbf{E} \parallel S$ ) and transverse ( $\mathbf{E} \perp S$ ) PE geometries described by the effective coefficients  $d_{EE}^S$  and  $d_{ES}^E$ . All figures are given in the units of pm/V.

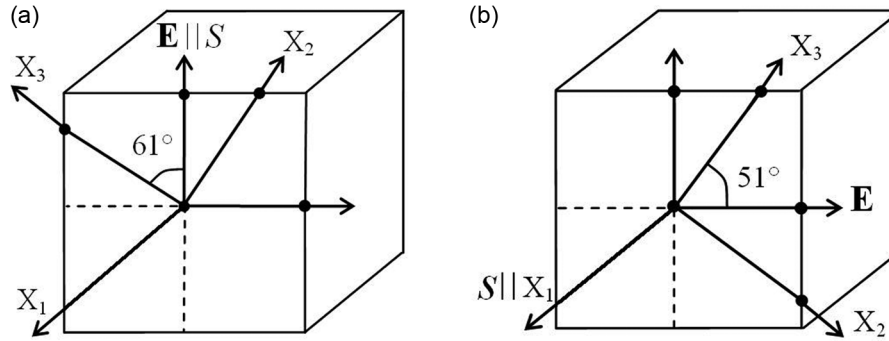


**Fig. 2** Optimal geometries of LiNbO<sub>3</sub>:MgO crystal samples providing the highest PE efficiency for the cases of longitudinal ( $\mathbf{E} \parallel S$ , panel (a)) and transverse ( $\mathbf{E} \perp S$ , panel (b)) effects, with indicated directions of electric field  $\mathbf{E}$  and induced PE strain  $S$ .  $X_1$ ,  $X_2$ ,  $X_3$  are the principal axes.

**Table 1** Extremal values of ISs for the PE and EO effects in LiNbO<sub>3</sub>:MgO and La<sub>3</sub>Ga<sub>5</sub>SiO<sub>14</sub> crystals, their angular orientation ( $\theta_0$  and  $\varphi_0$ ), and angular regions  $\delta\theta$  and  $\delta\varphi$  where the size of the effects is not less than 90 per cent from the extremal value, as found using the numerical techniques.

IS	Size of the effect, pm/V	$\theta_0$ , ang deg	$\varphi_0$ , ang deg	$\delta\theta$ , ang deg	$\delta\varphi$ , ang deg
Lithium niobate					
$d_{EE}^S$	38.2 (-38.2)	61 (119)	90, 210, 330 (30, 150, 270)	-12÷13	±15
$d_{ES}^E$	29.6 (-29.6)	129 (51)	90, 210, 330 (30, 150, 270)	-12÷11	±21
$d_{ES}^p$	19.2 (-19.2)	0, 180 (0, 180)	60, 180, 300 (0, 120, 240)	-18÷18	±9
$\delta\Delta_{EE}^i$	-531 (531)	50 (130)	90, 210, 330 (30, 150, 270)	-18÷14	arbitrary $\varphi$
$\delta\Delta_{Ej}^E$	-229 (229)	46 (134)	30, 150, 270 (90, 210, 330)	-18÷16	±15
Langasite					
$d_{ES}^p$	6.7 (-6.7)	15 (165)	30, 150, 270 (90, 210, 330)	-15÷17	±12
$\delta\Delta_{Ei}^E$	24.8 (-24.8)	126 (54)	30, 150, 270 (90, 210, 330)	-21÷20	±11

now that the optimal angular orientation of a sample is kept with respect to only one of the spherical angles (i.e., we have  $\theta = \theta_0$  and  $\varphi \neq \varphi_0$  or, vice versa,  $\theta \neq \theta_0$  and  $\varphi = \varphi_0$ ). Let us find the corresponding maximal allowed deviations (bandwidths)  $\delta\varphi$  or  $\delta\theta$  for the other angle, which ensure that the effective PE coefficient remains not less than 90 per cent of its extremal value. In case of the longitudinal effect (the IS  $d_{EE}^S$ ,  $\mathbf{E} \parallel S$ ), the allowed deviation  $\delta\theta$  in the polar angle is  $-12 \leq \delta\theta \leq 13^\circ$  when the  $\varphi$  angle is fixed at, e.g.,  $\varphi_0 = 90^\circ$ , whereas the bandwidth  $\delta\varphi$  for the azimuthal angle is equal to  $\pm 15^\circ$  when  $\theta = \theta_0 = 61.0^\circ$  or  $119.0^\circ$  (see table 1).

Notice that the positive and negative azimuthal deviations are always equal to each other. This is a result of symmetry of the ISs, which has to involve all the symmetry elements of the class  $3m$  characterizing lithium niobate (i.e., a three-fold axis  $X_3$  and three mirror planes intersecting at this axis). At the same time, the positive and negative polar deviations  $\delta\theta$  are asymmetric. Indeed, with the angles as large as  $\sim 10 \div 20^\circ$ , we leave a relatively narrow angular vicinity of an extremum point  $\theta_0$  where the curve  $d_{EE}^S(\theta)$  is still symmetric and, moreover, there is no point symmetry element that would impose the  $d_{EE}^S(\theta)$  curve to be symmetric relative to the point  $\theta_0$ , except for the cases of  $\theta_0 = 0$  or  $180^\circ$  (see the results for the IS  $d_{ES}^p$  in table 1).

The case of transverse piezoelectricity (the IS  $d_{ES}^E$ , with  $\mathbf{E} \perp S$ ) is characterized by the figures  $\delta\theta = -12 \div 11$  at  $\varphi = \varphi_0 = 30^\circ$  and  $\delta\varphi = \pm 21.0^\circ$  at  $\theta = \theta_0 = 51.0^\circ$  or  $129.0^\circ$  (see table 1). Hence, the stability of the IS extrema with respect to the polar angle is almost the same in the both cases, although their azimuthal angular bandwidths differ by the factor of about 1.4. Of course, a more general and complicated practical situation can happen when a deviation from the optimal spatial direction of extremum has both  $\theta$ - and  $\varphi$ -components nonzero. Then the problem of finding relevant allowed angular deviations  $\delta\theta$  and  $\delta\varphi$  may be solved using the Wulff net.

Figure 3 shows the ISs of the EO effect in LiNbO<sub>3</sub>:MgO (panels (a) and (b)), their stereographic projections on the  $X_1X_2$  plane (panels (c)–(d)), and less detailed stereographic projections with the regions of angular stability marked (panels (e)–(f)). Here panels (a), (c), (e) and (b), (d), (e) correspond to the electro-induced optical path

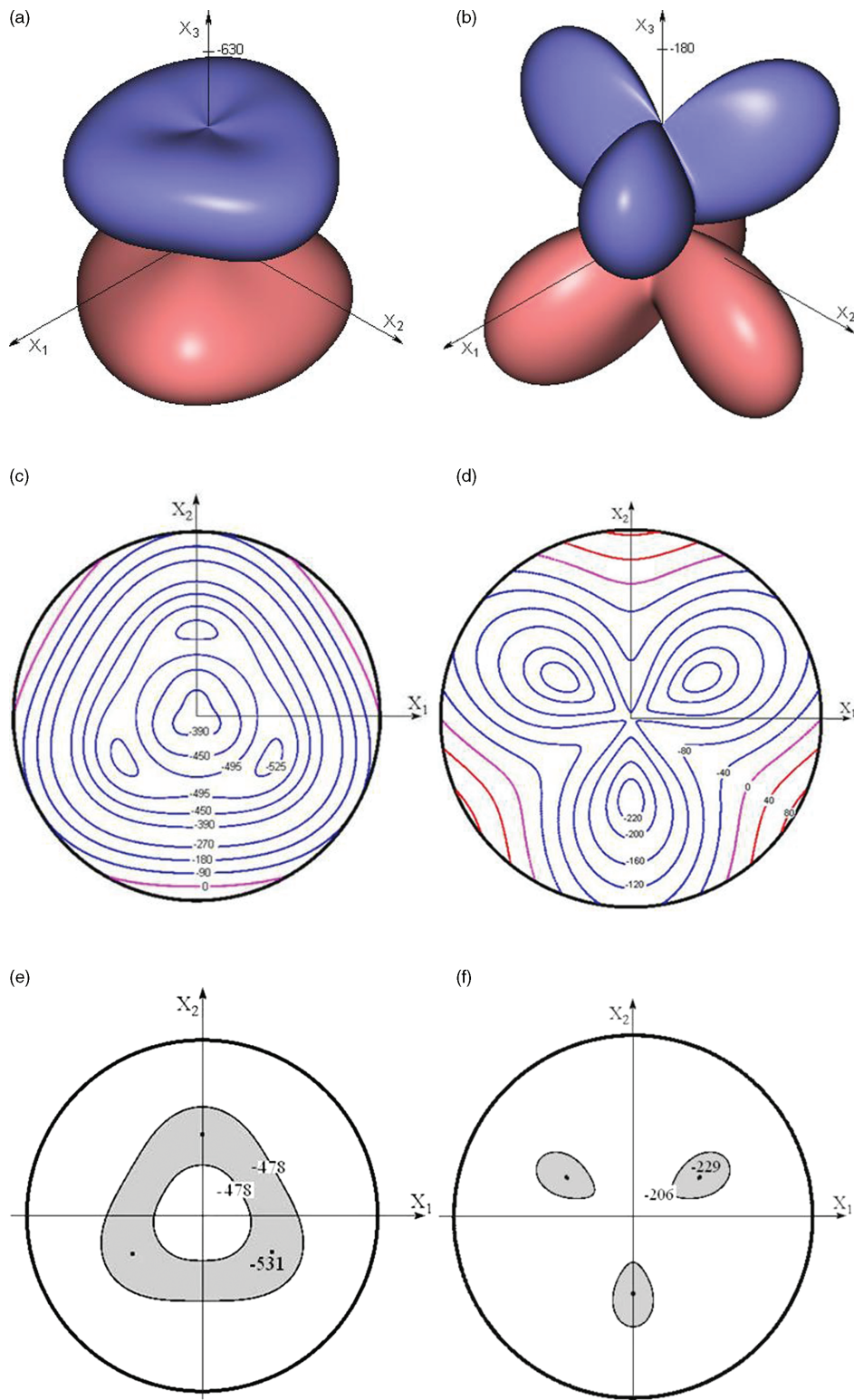


**Fig. 3** (a), (b) ISs of electro-induced optical path changes due to EO effect in LiNbO<sub>3</sub>:MgO crystals; (c), (d) their stereographic projections; (e), (f) stereographic projections with shaded angular bandwidths of the IS extrema (see explanations in text). Panels (a), (d), (e) and (b), (d), (f) correspond respectively to EO geometries described by the effective parameters  $\delta\Delta_{EE}^i$  and  $\delta\Delta_{Ej}^E$ . All figures are given in the units of pm/V.

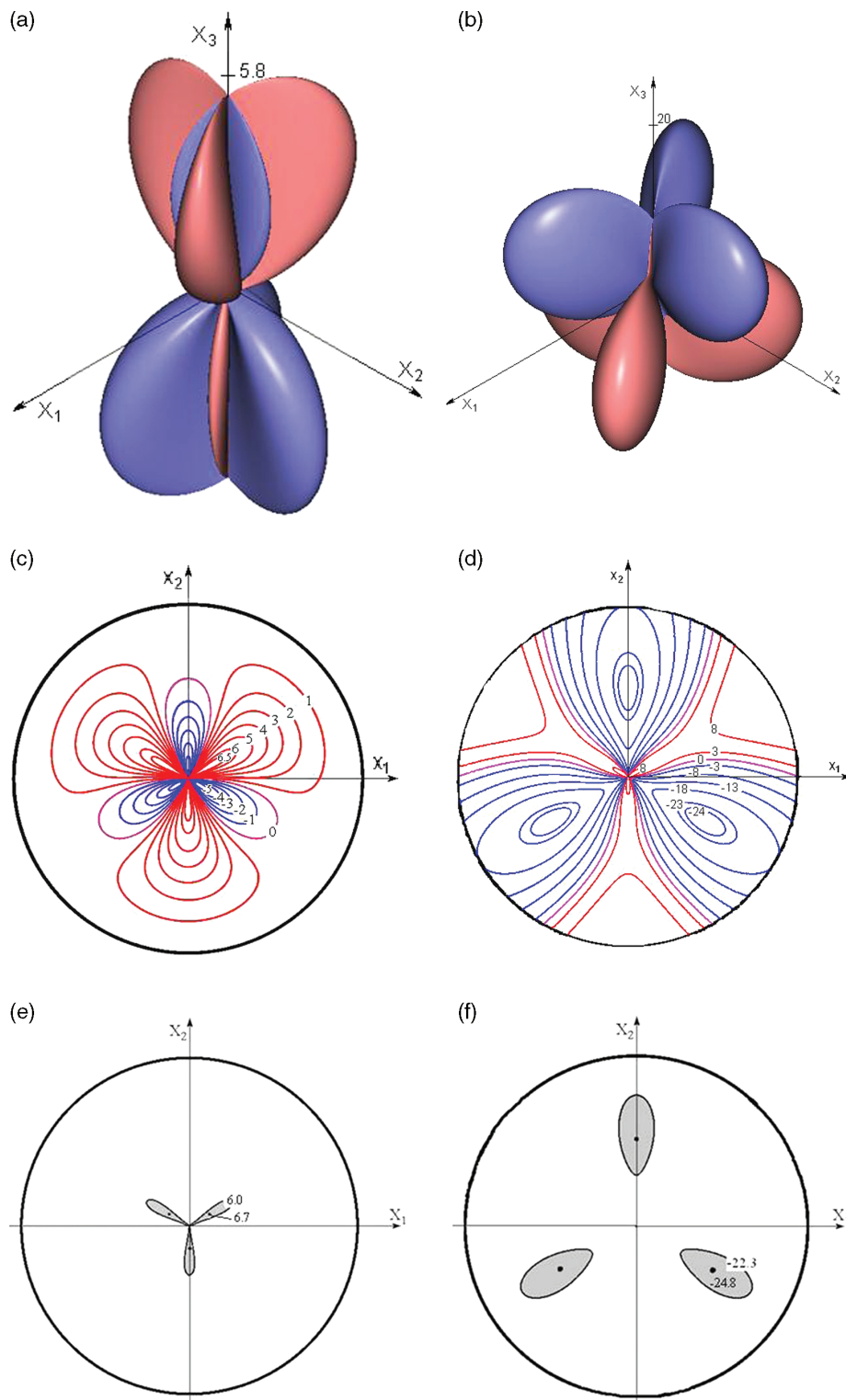


**Fig. 4** (a), (b) ISs of PE effect and electro-induced optical path changes due to EO effect in langasite crystals; (c), (d) their stereographic projections; (e), (f) stereographic projections with shaded angular bandwidths of the IS extrema (see explanations in text). Panels (a), (d), (e) and (b), (d), (f) correspond respectively to PE geometry described by the effective parameter  $d_{ES}^i$  and EO geometry described by the effective parameter  $\delta\Delta_{EI}^i$ . All figures are given in the units of pm/V.

changes  $\delta\Delta_{EE}^i$  and  $\delta\Delta_{Ej}^E$  appearing due to the transverse ( $\mathbf{k} \perp \mathbf{E}$ ) and longitudinal ( $\mathbf{k} \parallel \mathbf{E}$ ) EO effects, respectively. The regions shaded in panels (e) and (f) of figure 3 are again those in which the size of the effective EO parameters  $\delta\Delta_{EE}^i$  and  $\delta\Delta_{Ej}^E$  remains not less than 90 per cent of the extremal values. Here the main quantitative features of angular bandwidths of the extrema of the longitudinal EO effect are much the same as for the case of PE effect in lithium niobate (see figure 1 and table 1).

In case of the transverse EO effect, the deviation  $\delta\theta$  allowed for the polar angle reveals the largest asymmetry (from  $-18^\circ$  to  $+14^\circ$  – see table 1) associated with a peculiar shape of the IS  $\delta\Delta_{EE}^i$  (see also figure 3(b)). It is also interesting that, for the polar angle fixed at the optimal  $\theta_0$  value ( $\theta_0 = 50^\circ$  or  $130^\circ$ ) or in its vicinity, the size of the transverse EO effect does not depend at all upon the azimuthal angle  $\varphi$  (figure 3(e)). The appropriate crystal cut is characterized by both the largest size of the EO effect (see table 1) and extremely high angular stability and so it could be suggested for manufacturing EO cells. One can also remark that the angular optical aperture of those cells should be extremely wide. Of course, Eqs. (7), (8) and (10) defining the  $\delta\Delta$  parameters do not directly account for sample thickness changes happening when the light propagation direction deviates from the normal to crystal slab, although this effect can be compensated using sample surfaces of more intricate shapes. Finally, a comparison of angular bandwidth parameters of table 1 associated with the extrema of the PE and EO effects testifies that the latter effect is somewhat more stable.

Still more instructive is to compare the angular regions where the effect changes its size by less than 10 per cent for the cases of direct and nondirect crystal cuts. As examples, we have calculated the above ‘stability regions’ for the PE and EO ISs  $d_{EE}^S$  and  $\delta\Delta_{Ej}^E$  in the vicinity of the angular point  $\theta_1 = 90^\circ$  and  $\varphi_1 = 90^\circ$ , which corresponds to one of the direct cuts. Apart from notably less sizes of the effects ( $d_{EE}^S(\theta_1, \varphi_1) = 19.2^{\text{ii}}$  and  $\delta\Delta_{Ej}^E(\theta_1, \varphi_1) = 89.0$  – cf. with the relevant data of table 1), the ‘stability regions’ are equal only to  $\delta\theta = 1.6^\circ$ ,  $\delta\varphi = 8.6^\circ$  for the IS  $d_{EE}^S$  and  $\delta\theta = 1.8^\circ$ ,  $\delta\varphi = 8.6^\circ$  for the IS  $\delta\Delta_{Ej}^E$ . These values are essentially less than the bandwidths for the indirect cuts shown in table 1. In other words, those of the direct crystals cuts which do not correspond to the IS extrema are at a clear disadvantage when compared with the optimal nondirect cuts. The only drawback of the nondirect crystal cuts is obvious practical difficulties of their preparation and orientation.

**3.4 Numerical results for  $\text{La}_3\text{Ga}_5\text{SiO}_{14}$**  To illustrate spatial anisotropy of the PE and EO effects in langasite and angular bandwidths of their extrema, we have chosen only two examples, the IS  $d_{ES}^E$  of the transverse PE effect and the IS  $\delta\Delta_{Ei}^i$  of the EO effect linked with the electro-induced optical path changes (see Eqs. (9) and (10)). As for the necessary experimental data, we have used the PE coefficients  $d_{11} = -6.3$  and  $d_{14} = 3.7$  pm/V [25], the EO coefficients  $r_{11} = 2.63$  and  $r_{41} = -1.86$  pm/V [25], and our data for the refractive indices ( $n_o = 1.8988$  and  $n_e = 1.9117$ ) at the room temperature and the light wavelength 633 nm.

Figure 4 shows the mentioned ISs (panels (a) and (b)), their stereographic projections on the  $X_1X_2$  plane (panels (c)–(d)), and the same projections with angular bandwidths of the extrema marked (panels (e)–(f)). The relevant quantitative parameters are gathered in table 1. As above, we have assumed the optimal experimental geometry to be kept exactly with respect to one of the spherical angles, while the deviation (i.e., orientation error) to be concerned with the other angle only. As follows from the corresponding  $\delta\theta$  and  $\delta\varphi$  data shown in table 1, the angular bandwidths of the extrema of both the PE and EO properties of langasite are comparable in their magnitude and quite similar to the relevant data reported above for the lithium niobate doped with MgO. In other words, we have some grounds to believe that the angular bandwidths of the spatial extrema of the electric field-induced effects in different crystals should be similar and always very wide.

Notice also that the indirect crystal cuts of langasite, which are characterized by both the highest efficiency and a wide angular bandwidth of extremal values of the induced effects, can find their applications related to efficient PE energy conversion and EO coupling. In this relation, high angular stability of the effect size is of a primary practical importance, if one reminds of inevitable errors in orientation and manufacturing of crystals samples for the PE or EO cells.

## 4 Conclusions

In this work we have analyzed the ISs describing spatial anisotropy of external field-induced physical effects in crystals and the angular bandwidth of those ISs in the vicinity of their extrema, with especial emphasis on the PE

<sup>ii</sup>We are to remark that the ISs  $d_{ES}^E(0^\circ, 60^\circ)$  (see table 1) and  $d_{EE}^S(90^\circ, 90^\circ)$  acquire the same value 19.2 pm/V, which is nothing but the PE coefficient  $d_{22}$  for the lithium niobate doped with MgO (see Eqs. (4) and (6)).

and EO effects. A general theoretical approach is presented that considers the width of the mentioned extrema as a function of spatial orientation angle  $\alpha$  of the field (or laser beam), the temperature  $T$  of crystalline material, and the frequency  $\omega$  of the field (or light). The angular, temperature and frequency dispersive coefficients are introduced that characterize quantitatively the behavior of the effects when the parameters  $\alpha = (\theta, \varphi)$ ,  $T$  and  $\omega$  change.

The angular stability of spatial extrema of the electric field-induced effects is analyzed in more detail, using both the analytical and numerical techniques. The specific examples worked out by us include a canonical lithium niobate (LiNbO<sub>3</sub> doped with MgO for increasing laser irradiation hardness) and a less known La<sub>3</sub>Ga<sub>5</sub>SiO<sub>14</sub> (langasite) crystal. The ISs of the effective PE coefficient and the electrically induced optical path change due to EO effect have been dealt with. A number of optimal geometries for the PE and EO effects are listed, which enable constructing the most efficient PE and EO cells for opto- and acoustoelectronics, using lithium niobate and langasite crystals.

We have shown that the experimental geometries associated with the extrema of the ISs reveal a significant advantage. Namely, the changes in the effect size turn out to be noncritical with respect to angular deviations of the orientations of electric field, wave vector and polarization of light. The angular bandwidths of the IS extrema associated with one of the spherical angles (azimuthal or polar) are shown to be as wide as  $\sim 20 \div 40^\circ$ , provided that the other angle (polar or azimuthal) is fixed at an optimal value corresponding to the extremal effect size. This conclusion has been testified to be at least qualitatively independent of a crystalline material (LiNbO<sub>3</sub>:MgO or La<sub>3</sub>Ga<sub>5</sub>SiO<sub>14</sub>) and a field-induced effect (PE or EO) under test. In particular, if a case of optical effects is dealt with, this would mean an extremely wide angular aperture of EO devices based upon the nondirect cuts of crystalline materials.

As a consequence, the data of our analytical and numerical analyses for the both examples of crystals (see table 1) show that the experimental geometries associated with the extrema of anisotropic electric field-induced effects are definitely superior to all of the other geometries. In addition to the best performance characteristics linked to the size of the effect, they manifest unprecedented angular stability of that effect size, which is almost one order of magnitude higher than that peculiar for the 'direct crystal cuts' not revealing the IS extrema. Since in the majority of cases the extrema of the ISs correspond just to the indirect crystals cuts, the latter should manifest serious advantages over the direct crystal cuts. This situation may be compared to a drastic difference between the cases of usual and noncritical phase matchings for the nonlinear optical frequency conversion processes.

**Acknowledgement** The authors acknowledge numerous fruitful discussions with Professor A. V. Kityk (Czestochowa University of Technology, Poland). One of the authors (A. S. A.) acknowledges a Marie Curie International Incoming Fellowship within the 7<sup>th</sup> European Community Framework Programme (project N°272715).

## References

- [1] L. Bohatý, *Zeit. Kristallogr.* **194**, 235 (1991).
- [2] B. G. Mytsyk, Ya. V. Pryriz, and A. S. Andrushchak, *Cryst. Res. Technol.* **26**, 931 (1991).
- [3] A. S. Andrushchak, B. G. Mytsyk, and O. V. Lyubych, *Ukr. Fiz. Zhurn.* **37**, 1217 (1992).
- [4] O. G. Vlokh, B. G. Mytsyk, A. S. Andrushchak, and Ya. V. Pryriz, *Crystallogr. Rep.* **45**, 138 (2000).
- [5] V. M. Kedyulich, A. G. Slivka, E. I. Gerzanich, A. M. Guivan, and P. M. Lukach, *Condens. Matter Phys.* **6**, 271 (2003).
- [6] A. S. Andrushchak, Ya. V. Bobitski, M. V. Kaidan, B. V. Tybinka, A. V. Kityk, and W. Schranz, *Opt. Mater.* **27**, 619 (2004).
- [7] I. Martynyuk-Lototska, T. Dudok, Ya. Dyachok, Ya. Burak, and R. Vlokh, *Ukr. J. Phys. Opt.* **5**, 67 (2004).
- [8] P. Han, W. Yan, J. Tian, X. Huang, and H. Pan, *Appl. Phys. Lett.* **86**, 052902 (2005).
- [9] M. V. Kaidan, B. V. Tybinka, A. V. Zadorozhna, W. Schranz, B. Sahraoui, A. S. Andrushchak, and A. V. Kityk, *Opt. Mater.* **29**, 475 (2007).
- [10] A. Say, O. Mys, A. Grabar, Yu. Vysochanskii, and R. Vlokh, *Phase Trans.* **82**, 531 (2009).
- [11] A. S. Andrushchak, B. G. Mytsyk, N. M. Demyanyshyn, M. V. Kaidan, O. V. Yurkevych, S. S. Dumych, A. V. Kityk, and W. Schranz, *Opt. Las. Eng.* **47**, 24 (2009).
- [12] A. S. Andrushchak, E. M. Chernyhivsky, Z. Yu. Gotra, M. V. Kaidan, A. V. Kityk, N. A. Andrushchak, T. A. Maksymyuk, B. G. Mytsyk, and W. Schranz, *J. Appl. Phys.* **108**, 103118 (2010).
- [13] J. F. Nye, *Physical Properties of Crystals: Their Representation by Tensors and Matrices* (Oxford University Press, Oxford, 1985).

- [14] B. G. Mytsyk, A. S. Andrushchak, M. N. Demyanyshyn, Y. P. Kost', A. V. Kityk, P. Mandracci, and W. Schranz, *Appl. Opt.* **48**, 1904 (2009).
- [15] A. S. Andrushchak, B. G. Mytsyk, H. P. Laba, O. V. Yurkevych, I. M. Solskii, A. V. Kityk, and B. Sahraoui, *J. Appl. Phys.* **106**, 073510 (2009).
- [16] Yu. S. Kuzminov, *Electro-Optical and Nonlinear Optical Lithium Niobate Crystals* (Nauka, Moscow, 1987).
- [17] I. A. Andreev, *Zhurn. Tekhn. Fiz.* **74**(9), 1 (2004).
- [18] B. G. Mytsyk, N. M. Demyanyshyn, A. S. Andrushchak, Ya. P. Kost', O. V. Parasyuk, and A. V. Kityk, *Opt. Mater.* **33**, 26 (2010).
- [19] V. G. Dmitriev and L. V. Tarasov, *Applied Nonlinear Optics, Radio i sviaz'* (Moscow, 1982).
- [20] H. Liao, H. Shen, Z. Zheng, T. Lian, Y. Zhou, C. Huang, R. Zeng, and G. Yu, *Opt. Lasers Technol.* **20**, 103 (1988).
- [21] T. Ukachi, R. J. Lane, W. R. Bosenberg, and C. L. Tang, *Appl. Phys. Lett.* **57**, 980 (1990).
- [22] J. T. Lin, J. L. Montgomery, and K. Kato, *Opt. Commun.* **80**, 159 (1990).
- [23] J.-Q. Yao, Y.-Z. Yu, P. Wang, T. Wang, B.-G. Zhang, X. Ding, J. Chen, H. J. Peng, and H. S. Kwok, *Chin. Phys. Lett.* **18**(9), 1214 (2001).
- [24] W. Brunner and K. Junge, *Wissenspeicher Lasertechnik* (Fachbuchverlag Leipzig, Leipzig, 1987).
- [25] O. V. Yurkevych, B. G. Mytsyk, and A. S. Andrushchak, *Proc. 10<sup>th</sup> International Conf. TCSET'2010, Lviv–Slavske (Ukraine) 2010*, p. 335.
- [26] A. S. Andrushchak, B. G. Mytsyk, N. M. Demyanyshyn, M. V. Kaidan, O. V. Yurkevych, I. M. Solskii, A. V. Kityk, and W. Schranz, *Opt. Lasers Eng.* **47**, 31 (2009).
- [27] O. V. Yurkevych, I. M. Solskii, and A. S. Andrushchak, *Herald of Lviv Polytechnic National Univ., Ser. Electronics* **646**, 147 (2009).